9-2018

Underwater adhesive using solid–liquid polymer mixes

Alin Cristian Chipara

T. Tsafack

P. S. Owuor

J. Yeon

C. E. Junkermeier

See next page for additional authors

Authors

Alin Cristian Chipara, T. Tsafack, P. S. Owuor, J. Yeon, C. E. Junkermeier, A. C. T. van Duin, S. Bhowmick, S. A. S. Asif, S. Radhakrishnan, and Mircea Chipara

Version of Record: https://www.sciencedirect.com/science/article/pii/S2468519418301423
Manuscript_48fb0b7a6404fbe2643ad73a1d0b7b6c

Underwater adhesive using solid-liquid polymer mixes

Alin Cristian Chipara[a,f], Thierry Tsafack[a], Peter Samora Owuor[a], JejoonYeon[b],Chad E. Junkermeier[b], Adri C. T. van Duin[b], Sanjit Bhowmick[c], S. A. Syed Asif[c], Sruthi Radhakrishnan[a], Jun Hyoung Park[6], Gustavo Brunetto[4], Benny Abraham. Kaipparettu[e,g], Douglas S. Galvão[d], MirceaChipara[e], J. Lou[a], Harvey H. Tsang[f], Madan Dubey[f], Robert Vajtai[a], Chandra Sekhar Tiwary[a*],and Pulickel M. Ajayan[a*]

[a]Department of Materials Science and Nano Engineering, Rice University, Houston, TX, 77005, USA

[b]Department of Mechanical and Nuclear Engineering, Penn State University, University Park, PA 16802, USA

[c]Hysitron, Inc., 9625 West 76th Street, Minneapolis, MN 55344, USA.

[d]Applied Physics Department, State University of Campinas – UNICAMP, 13083-859 - Campinas, SP – Brazil.

[e]Department of Physics and Geology, University of Texas-Rio Grande Valley, Edinburg, TX 78539, USA

[f]Department of Molecular and Human Genetics, Baylor College of Medicine, Houston, Texas 77030, USA

[f]U. S. Army Research Laboratory, Sensors and Electron Devices Directorate, 2800 Powder Mill Road, Adelphi, Maryland 20783, USA

[g]Dan L. Duncan Cancer Center, Baylor College of Medicine, Houston, TX 77030 (USA)

Abstract

Instantaneous adhesion between different materials is a requirement for several applications ranging from electronics to biomedicine. Approaches like surface patterning, chemical cross-linking, surface modification, and chemical synthesis have been adopted to generate temporary adhesion between various materials and surfaces. Because of the lack of curing times, temporary adhesives are instantaneous, a useful property for specific applications that need quick bonding. However, to this day, temporary adhesives have been mainly demonstrated under dry conditions and do not work well in submerged or humid environments. Furthermore, majority rely on chemical bonds to form strong interaction with their substrates like acrylate-based. This work demonstrates the synthesis of a universal amphibious adhesive solely by combining solid

polytetrafluoroethylene (PTFE) and liquid polydimethylsiloxane (PDMS) polymers. While the dipole-dipole interactions are induced by a large electronegativity difference between fluorine atoms in PTFE and hydrogen atoms in PDMS, strong surface wetting allows the proposed adhesive to fully coat both substrates and PTFE particles, thereby maximizing the interfacial chemistry. The two-phase solid-liquid polymer system displays adhesive characteristics applicable both in air and water and enables joining of a wide range of similar and dissimilar materials (glasses, metals, ceramics, papers, and biomaterials). The adhesive exhibits excellent mechanical properties for the joints between various surfaces as observed in lap-shear testing, T-peel testing, and tensile testing. The proposed bio-compatible adhesive can also be re-used multiple times in different dry and wet environments. Additionally, we have developed a new reactive force field parameterization and used it in our molecular dynamics simulations to validate the experimental results of the adhesive nature of the mixed polymer system with different surfaces. This simple amphibious adhesive could meet the need for universal glue that performs well with a number of materials for a wide range of conditions.

Keywords: PDMS, PTFE, Glue, Electronegativity, Solid-liquid, Adhesive
E-mail: cst.iisc@gmail.com, ajayan@rice.edu

1. Introduction

Newer and simpler ways to generate adhesion in various materials have been the subject of several recent studies[1,2]. Several approaches have been used to achieve this including patterning, cross-linking, surface modification, and chemical synthesis[3–7]. Yuk et al[5] surface functionalized hydrogels to allow them to readily stick to porous surfaces. Mussel-derived proteins and 3,4-dihydroxyphenylalanine (DOPA) cross-linkers have also been used as water-resistant adhesives[5,7,8]. Research focused on patterning materials to create strong adhesive materials have shown impressive results, yet face scalability issues[9]. Many polymer adhesives rely on cross-linking or *in-situ* polymerization, which can lead to unexpected changes in material properties[1]. Adhesives derived from these methods can also suffer from substrate limitations, environmental limitations, long curing times, toxicity, and lack of recyclability. Furthermore, instant curing adhesives have become an area of growing interest to avoid the drawbacks associated with the curing process. To this day, the search for a versatile biocompatible adhesive with the ability to work in any humidity level, show reversibility, and have a myriad of substrate choices is an ongoing focus. Such an adhesive is extremely useful for biomedical, underwater, as well as energy applications. Unlike chemically crosslinked adhesives, natural underwater adhesives have high re-usability and multi-functionality. The present study proposes a solid-liquid adhesive system based on a combination of dipole-dipole interactions and surface wetting present in polymer mixes.

The adhesive is synthesized in easily scalable method from versatile readily available building blocks which are re-usable, biocompatible, and can work underwater. The adhesive can work with a myriad of substrates and avoid harmful side reactions generally associated with covalently cross-linked adhesives[10]. The adhesive is based on Flourine (F) - Hydrogen (H)

electronegativity difference and mechanical interactions between solid and liquid phase. As the polymers mix, the PDMS chains re-orient themselves and, due to the large electronegativity difference between the F atoms on PTFE and H atoms in PDMS, dipoles are induced between the two polymer chains, which give rise to adhesive properties. The non-toxicity nature of the adhesive, makes it a valuable one to be used in medical application where instantaneous adhesion under moist conditions in highly needed.

2. Experimental Section

Equal weight of hydroxyl terminated PDMS (Sigma Aldrich 18,000-22,000 cSt) and PTFE (DuPont Zonyl 1000 MP submicron particles) were measured out using a digital scale and then mixed with a metal spatula (by hand) until a homogenous mixture was obtained. PTFE Zonyl MP 1000 is powder comprising of average 100nm sized particles. 90% of particles are found to be 100nm. Additionally, they have a specific surface area of 5-10 m^2/g. The density of PDMS (0.96gm/cc) and PTFE (2.2 gm/cc) are considered for calculating volume-fraction which turns out to be 2/3 of PDMS and 1/3 PTFE. In current work, we have synthesized mixture of different weight ratio (1:2, 1:1, 2:1 for PDMS:PTFE), the 50% (1:1) is found to be optimum, hence all results are based on his ratio.

Qualitative tests were performed using standardized weights. The substrates were all cut to the same size, except for the Si wafer. The adhered area was 25 mm by 25 mm for all samples apart from Si (which was 12.94 mm by 10.84 mm). All calculations for stress were done using $\sigma = F/A$. The materials all had a glue thickness of 0.1 mm. All size measurements were done with digital calipers. The materials were not polished but were cleaned in between each test that didn't test re-usability. Each material was cleaned using an IPA wipe and the glue was applied using a

metal spatula. The materials were tested by taping weights to the bottom of the substrates after adhesion and holding at 90^{o} for several minutes as shown in the supplemental material. The submersed tests were one by sticking already glued materials underwater. This was separately verified by taking two pieces of copper with glue on them and pressing them together underwater, which also led to adhesion. The raw weights that each sample could hold were 350 g, 150g, 150 g, 100g, and 30g for Paper, Cu foil, glass, plastic, and Si wafer, respectively.

Dynamic Mechanical Analysis Testing.
DMA testing was performed at 0.1N/min and 0.001N/min for pure PDMS, 25% PTFE/PDMS and 50% PTFE/PDMS. The testing was performed in force controlled mode in tensile using samples made of copper foil (overall size ~18 mm x 6 mm, length x width). The testing was performed at standard room temperature and pressure.

Quantitative Mechanical Tensile Test.
The tensile testing was performed using an ADMET eXpert 7600 setup with a steel wire to pull at 90^{o}. The steel wire was attached to a hook that was directly welded into the upper metal substrate used in the adhesion. The pulling was performed at a rate of 5 mm/min. We tested both adhesion between two metal substrates and adhesion between a plastic (polycarbonate) and aluminum substrate. For the adhesion between mismatched substrates, we replaced the bottom aluminum piece with a piece of plastic and repeated the same procedure. The procedure was repeated several times without re-application of the adhesives and without touching the adhesive surface. The procedure was also repeated after smoothing out the adhesive surface in between runs, but after failure.

In-Situ SEM Testing.
In-situ testing was performed at Hysitron Inc. PI85 indenter attached inside 3D VERSA with field emission gun.

FTIR and TGA Thermal Characterization.

FTIR was performed at the Army Research Laboratory. (Thermo Nicolet Nexus 670) using an averaging of 16 scans per spectrum with a resolution of 4 cm^{-1}. The material was spread between salt crystal wafers and scanned with varying PTFE: PDMS ratios. TGA was performed using a TGA 500. The procedure was performed in air up to 800^{o}C at a rate of 10^{o}C/min.

X-Ray CT Measurements.

When trying to produce high quality CT scans, the sample preparation can be as critical as the scanning process. The sample was mixed and applied onto a 25 mm by 25 mm glass slide, an identical slide was pressed against the sample and then pulled apart, taking care to not add any sliding or rotation to this process. The glass slide was then mounted into the Zeiss Xradia 510 Versa so that at 0° the source and detector would be at a normal to the plane of the glass slide. To enhance phase contrast for edge detection, the source and detector were brought in as close to the sample as possible, without collision during its rotation from 0 – 360 °. The recipe was set to 80kV, 7W, 4X objective, no filter, 0.5 second exposure with 8601 projections and multiple references. All CT measurements and analysis was done at the Adelphi Laboratory Center (ALC).

T-Peel Testing.

The T-peel test was performed on an Instron 5500R test frame with a 50 lb load cell at the Army Research Lab in Aberdeen Proving Ground (ARL-APG). The testing used tensile grips. The adhesion substrates were cut into 1 inch by 4 inch sizes from a new sheet of Dura-Lar Grafix polyester. The samples were manually cleaned using wipes to remove any particulates from the surface. The substrate thickness was measured using calipers and found to be 0.004 inches. It is important to note that we had to change the ratios for the SiO2 samples since the saturation limit for them was much lower compared to PTFE. The material was smeared onto a 3 inch by 1 inch adhesion area (leaving 1 inch as the gripping region). Afterwards, a second sample was placed

on top and we rolled a steel cylinder over the top of the sample to apply uniform pressure to the substrates and adhere them. There were 5 T-peel test samples made for each composition and control. The adhesive thickness (Adhesive thickness = Sample thickness - 2(polyester sheet thickness)) was measured for each sample and noted. The samples were then mounted into the grips by placing the unadhered area into the grip jaws and tightly gripping them and separated at a rate of 254 mm/min (1 in/min). The extension and force were measured directly through the built-in software. The sample then underwent the same testing method as the other adhesive samples. The average adhesive thickness was ~0.003 in/ 0.0762 mm. All samples exhibited cohesive failure after being peeled apart.

Computational Details.

All mechanical properties are computed using classical molecular dynamics (MD) with its numerical implementation in the large-scale atomic/molecular massively parallel simulator[11] (LAMMPS), using: 1) the parameterizations of the Reax Force Field (ReaxFF) described below, 2) a timestep of 0.25 femtoseconds, and the 3) Nosé-Hoover thermostat at room temperature.

The ReaxFF C/O/H/Si/F force field parameters used in this work are a combination of the carbon-parameters from Srinivasan *et al*[12]. which were extended to C/H/O interactions by training against the DFT-data described by Chenoweth and co-workers[13]. The Si/C interaction parameters were trained against the DFT-training set described in the PDMS/ReaxFF work [14]. The new C-F bond and affiliated angle and dihedral terms were trained against DFT-data derived from a Zdol-monomer (Fig.S2a, Supporting information) and from $(H_3C)_2CF_2$, C_4F_{10} and F_2 molecules. All DFT calculations were performed at the B3LYP/6-311G** level. Supporting information S2b-d compare the ReaxFF and DFT results for the bond, angle and dihedral scans for the training set molecules. Overall, the ReaxFF performance is a good match to the DFT-data. The ReaxFF bond energies are typically a little lower than the DFT-numbers – but as such

provide a better match to experimental bond energies. For the C-O-C angle in Zdol, ReaxFF obtains a shallow secondary minimum at around 90 degrees – this is probably due to the formation of a weak C---C bond across the C-O-C angle; this could potentially be repaired by increasing the C-C-O angle parameter force constants. However, this secondary minimum is quite shallow (about 1 kcal/mol) and as such is not expected to significantly affect C-O-C angle behavior during MD-simulations. In Fig. 1d, we only show the dihedral angle cases with meaningful rotational barriers; we also performed DFT analyses for the C-O-C-O and C-C-O-C dihedrals in Zdol and found very small rotational barriers (< 0.5 kcal/mol) – and these small barriers are reproduced by ReaxFF.

Single units of hydroxyl-terminated PDMS, $OH\text{-}[Si(CH_3)_2O]_n\text{-}H$, and PTFE, $(C_2F_4)_m$, with n = 410 and m = 512, were prepared using the molecule editor Avogadro[15], equilibrated in a canonical ensemble (NVT), in a 150 Å × 150 Å × 150 Å simulation box with fixed boundary conditions, for 40 picoseconds. The equilibrated PDMS and PTFE units (see Fig.S21a-b, Supporting information) were inserted into two 100 Å × 100 Å × 100 Å simulation boxes with periodic boundary conditions. The PDMS+PTFE box contained three PDMS units and one PTFE unit while the PDMS box contained three PDMS units. Both boxes were squeezed by roughly 20% in a microcanonical ensemble (NVE) for 5 picoseconds and equilibrated first in a canonical ensemble (NVT) for 5 picoseconds to ensure an even distribution of particles in the box and then in an isothermal-isobaric ensemble (NPT) for 5 picoseconds to relax the simulation box. This series of equilibration processes resulted in a 51 Å × 51 Å × 51 Å PTFE/PDMS simulation box with a mass density of ~1.8 g/cc and a 20 Å × 20 Å × 20 Å PDMS simulation box with a mass density of ~0.97 g/cc (see Fig. S11a). Further, a 1 × 1 × 2 PTFE/PDMS supercell was then sandwiched between two identical 76 Å × 108 Å × 11 Å bulk Si (100) substrates into two

configurations: A configuration (Si/Blend/Si) with the PTFE/PDMS supercell lying on the surface of the substrate and a configuration (Si/Blend+H_2O/Si) with the PTFE/PDMS supercell ~5Å away from the surface of the substrate (see Fig. 3). Water molecules, H_2O, were added into the second configuration in the space between the substrates and the PTFE/PDMS supercell as well as all around the PTFE/PDMS supercell until they reached the density of ~1 g/cc. They were then equilibrated in a canonical ensemble (NVT) for 30 picoseconds (with periodic boundary conditions) to ensure proper chemical interactions with the substrate and the mixture.

The computation of the stress-strain relationships on the above PTFE/PDMS, PDMS, Si/Blend/Si, and Si/Blend+H_2O/Si models proceeded by: 1) further equilibrating the respective structures in an isothermal-isobaric ensemble (NPT) while compressing them by 22%, 22%, 30% and 33% respectively for 5 picoseconds and 2) stretching them back by 25%, 25%, 33%, 35% respectively for 5 picoseconds. As the box compression/tension or loading/unloading occurred uni-axially (in the x, y, and z direction) and bi-axially (in both x and y directions), the respective stresses and strains at every step were computed. Simulating a large PTFE sphere with PDMS surrounding it in MD would take a very large amount of computing power and time, hence the sizes are scaled down as per real system.

Computational Details (Ab initio).

PDMS, $(C_2H_6OSi)_n$, and PTFE, $(C_2F_4)_m$, structures in Figures 3b-d are constructed with n = 3, m =3, and with hydrogen passivation of both ends of both trinomers. Both trinomers were optimized using the all-electron density functional theory (DFT) equations implemented in the Gaussian 09 package[16] with the B3LYP functional of generalized gradient approximation[17] and the 6-31G basis set[18].The threshold convergence criteria for the root-mean-square (RMS) force, maximum displacement of atoms, the maximum force, and RMS displacement are set to 0.0003, 0.0018, 0.00045, and 0.0012a.u., severally. The electrostatic potentials along with the

highest occupied (HOMO) and lowest unoccupied (LUMO) molecular orbitals for the considered PDMS and PTFE trinomers are extracted for further analyses. The electrostatic potentials are depicted in a range of -0.002 to 0.002 Mulliken units, the redder the area, the more negative the charge, the bluer the area, the more positive the charge.

Biocompatibility Testing.
MDA MB 231 cells were cultured in a 96 well plate. 2000 cells were seeded in each well. The specified amount of glue was dissolved in the cell culture media by mechanical mixing. Various concentrations were then added to the cells in culture. The cells were incubated for 24 hours and 48 hours. After the incubation time the media was aspirated and the cells were washed with PBS before adding the MTT reagent. The cells were incubated with the MTT reagent for 2 hours before adding DMSO as the stop solution. The absorbance was then measured in a plate reader. There was no significant cell death observed at concentration as high as 1mg. The experiment was repeated with higher concentrations (5mg, 10mg) of the material. However, no significant toxicity or cell death was observed. To study the growth of the cells on the glue, it was well spread uniformly on the cell culture dish. This was incubated with the media for a day before adding the cells. The study was conducted on GFP labelled human embryonic cell line HEK 293T and GFP labelled breast cancer cell line MDA MB 231. No cell growth defects were seen.

3. Results and Discussion

To analyze the potential of dipole-induced adhesion, we chose to synthesize a blend using hydroxyl terminated PDMS (poly dimethylsiloxane, liquid phase) and PTFE (polytetrafluoroethylene, solid phase). The fluorine content in PTFE is capable of generating an induced dipole-moment in neighboring atoms [19,20]. The solid spherical PTFE particles that were used (DuPont Zonyl 1000 MP) were ~100nm in radius, with a large surface area (See Fig.

S2 Supporting information for SEM images). As mixing occurs, PDMS organizes preferentially around PTFE spheres (Figs. 1a, b, and d). The molecular-level dipole interactions repeat many times per polymer chain and give rise to macro-scale adhesive properties. During shear/torsion, PTFE is attracted to PDMS due to dipole interactions and resist deformation (Fig. 1a). Additionally, during tension the dipole interactions attempt to hold PTFE in place (Fig. 1b). The adhesion does not exploit chemical bonds or interactions; the approach is essentially based on physical interactions among atoms/molecules (dipole-dipole induced interactions) and molecular flexibility (of PDMS). Hence no additional chemical groups have been involved or have been considered relevant for the type of adhesion described in this manuscript.

Under SEM, the 1:1 PTFE/PDMS blend showed a homogenous polka-dot pattern (Supporting information S2a-c). To the naked eye, the material looks like a white gel, whereas, PDMS is clear and PTFE is a white powder (inset in Fig. 1c). SEM images after tensile failure (Fig. 1c) show that PTFE tends to pull out of the PDMS matrix. This is further supported by the stress lines that can be seen around the pullout area (see inset in Fig. 1c). In comparison, shear failure (shown in Fig. 1e) shows stress lines developing around the PTFE particle, which indicates that PTFE spheres act as areas of concentrated stress (as indicated by the strain lines in the inset in Fig. 1e and Fig. S3, Supporting information).

In-situ mechanical measurements attached to SEM show stringing within the PTFE/PDMS blend. Stringing is a characteristic of adhesives, appearing as the adhesives' attempts to keep both substrates adhered (Figs. 1f-h) [21]. The *in-situ* tensile test is shown in a series of SEM images that correspond to compressive pre-loading, loading (in tension), and unloading (Figs. 1f, g, and h, respectively). The *in-situ* load-displacement curve shows full recovery after each cycle but some distinct abnormalities are present in the first cycle (Fig. 1i).

The material does not exhibit residual strain and shows recoverable cyclic behavior, which indicates no loss of adhesion over several cycles. The recoverability is complemented by the liquid phase, which prevents crack formation and propagation.

The chemical structure of the material was analyzed using FTIR spectroscopy, as seen in Fig. S4a in supporting information. The analysis confirms absence of any new chemical bonds, thus eliminating the possibility of covalent bonding within the blend. As we change concentration of PTFE, CF_2 peaks appear and the relative intensity of PDMS decreases (Fig.S4a, Supporting information).[22–25] Thermogravimetric analysis (TGA), performed in air at 10^oC/min, supports the spectroscopy data (Fig.S4b, Supporting information). Additionally, the TGA data indicates the presence of molecular interactions as exhibited by the shift in degradation temperature by ~80^oC, relative to pure PDMS[26,27].

To quantify the strength of the adhesive bonds we used dynamic mechanical analysis (DMA) for shear measurements (Fig. 1k), in tandem with tensile testing (Fig. 1l). Shear testing was performed using a force-controlled method at a rate of 0.1 N/min and 0.001 N/min. The rate plays a very important role in the apparent strength of the material, as lower rates will exhibit lower strength. At 0.1 N/min, the adhesive showed a maximum strength of ~0.3 MPa before exhibiting cohesive failure (see Fig. 1k). This is an increase of 548% over pure PDMS, which was also tested at 0.1 N/min (see Fig. 1k and the corresponding inset). Under a slower rate (0.001 N/min), the adhesive showed a 5,800% increase over pure PDMS that was tested at the same rate (see inset in Fig. 1k). DMA results also showed a stark difference between having 25 wt.% PTFE and 50 wt.% PTFE in the sample (Fig.S5, Supporting information). The data shows that even 25% PTFE content shows a nominal increase in adhesion compared to PDMS (also shown in peel testing in Fig.S6, Supporting information), however, using 50% PTFE shows a

524% increase (in relation to a 25% PTFE/75% PDMS blend). This implies that the fluorine atoms in PTFE play a large role in the adhesive behavior. While filler geometry plays a role in the adhesion properties of PDMS, a comparative test using similar sized particles and concentrations of SiO_2/PDMS and PTFE/PDMS shows that SiO_2 does not enhance the adhesion as much as PTFE (Fig.S7, Supporting information). This implies that the adhesion mechanism is a mixture of both chemical and mechanical effects but is more reliant on chemical interactions (dipole-dipole, electrostatic).

The failure pattern (Fig. 2a) shows aggregations in the direction of failure (also seen in Supporting information Figs. S8a-f). In the case of shear failure, the surface pattern (Fig. 2a) and SEM images (Fig. 1e) indicate that failure occurred due to PTFE spheres slipping past each other in the PDMS matrix (cohesive failure). To complement the shear testing, tensile testing was performed using an ADMET testing system. The testing was performed by adhering a 25.5 mm aluminum disk onto an aluminum block (using the PTFE/PDMS blend) and pulling at a rate of 5mm/min (see Fig. 1l and Fig.S9, Supporting information). The test was repeated for PDMS, and with mismatched substrates (aluminum and plastic, with more substrates shown in Supporting information Figs. S10a-b). The blend showed a 3408% increase over PDMS in loading mismatched materials and an 1814% increase in loading aluminum samples (highlighted in the inset in Fig. 1l). The strongest adhesion was seen using aluminum substrates and the failure mode can be seen in Fig. 2b. The failed samples exhibited cohesive failure and ridge-like adhesive residue patterns on the surface (Fig. 1c).

One of the most important properties of adhesives or adhesive-like materials is their ability to adhere multiple types of substrates under varying environments (Figs. 2c-d). Our observations show that once a drop of PTFE/PDMS is put on the surface of a copper sheet, it

spreads out over time, thus causing the contact angle to change (Figs. 2e-g). This is a specific advantage of the liquid phase of the mixture. Thanks to the high mobility of the PDMS chains, the material can freely enter pores and fill them, thus allowing it to fully wet surfaces and enable good adhesion (Supporting information Figs. S10g-l). Moreover, this material exhibits hydrophobic properties (Fig. 2g) which allows it to function underwater while still being able to wet many different types of surfaces. The wettability of the material was probed using SEM to image the interface between the PTFE/PDMS materials and copper/paper. SEM images showed that the PTFE/PDMS material fully coats both copper (Fig. 2h) and paper (Fig. 2i), thus eliminating surface features and fully cover the substrate surface and pores. This is schematically explained in Fig. 2j. We believe that the ability of the adhesive to drive the water layer away comes from its intrinsic hydrophobic nature. Numbers of experiments have demonstrated the hydrophobic nature of PDMS and PTFE separately, and since there is no covalent bonding between the two polymers, we are inclined to assume that the combination of PDMS and PTFE conserve their respective hydrophobic tendencies. To further highlight this important chemical property of the adhesive, we have analyzed the reactivity between water molecules and PDMS/PFTE units on the basis of the Fukui frontier molecular orbital theory (FMOT).

Within the FMOT framework, chemical affinity mostly occurs because of constructive HOMO-LUMO or LUMO-HOMO molecular orbital overlap, which means that the biggest coefficients of the same sign (blue or red color) of the wave function from frontier orbitals belonging to atoms in the two reactants, should easily overlap. In Fig.S11, Supporting information(top), the interaction between water molecule and PDMS must proceed from the HOMO of water to the LUMO of PDMS because O (red atom) in water is more of an electron donor than either H (white atom) or C (black atom) in the sticking methyl group of PDMS. The

two big coefficients around O do not click with any single pair of coefficients around either H or C in the PDMS unit. The experimental hydrophobic nature of PDMS is thus confirmed by the poor affinity predicted within the FMOT framework. Similarly, since the sticking F (aqua blue atom) in PTFE is more of an electron donor than O in water, the interaction must proceed from the HOMO of PTFE to the LUMO of the water molecule. Since the big red coefficient of the water LUMO surrounds the entire water molecule thus hiding the very small blue coefficient inside the molecule, it makes the orbital overlap practically impossible. The very little affinity between water molecules and PTFE units results in the hydrophobic property of PTFE. We have thus shown, with interactions at the frontier orbitals, that the proposed PDMS/PTFE adhesive exhibits very little affinity with water molecules.

The multifold improvement in the adhesive behavior of PDMS is due to molecular interactions between solid-liquid. To verify our hypothesis, we employed molecular dynamics simulations with ReaxFF (force field parameters described in the computational details section and Fig.S12, Supporting information). The theoretical calculations (schematically shown in Fig. 2k) revealed stress-strain relationships (Figs. 2l-o) very similar to those seen in the experimental testing (Figs. 1i-l, Supporting video V1). The data show that the blend has very strong cohesive and adhesive properties arising from the large electronegativity difference between the fluorine and hydrogen atoms (1.9). This is emphasized by the fact that the blend can recover from 20% compressive stress while PDMS cannot. The blend also exhibits much higher maximum stress at similar strain values compared to pure PDMS. During unloading, the PDMS easily separates out whereas the blend displays strong interfacial bonding which allows it to hold together up to 25% tensile strain (Figs.S13b-c, Supporting information). Hence PDMS units do not interact with each other strongly, unlike the PTFE/PDMS blend (Fig. 2k). Interfacial PTFE fluorine atoms are

therefore expected to attract interfacial PDMS hydrogen atoms thereby forming flexible, but strong PTFE-PDMS interfacial interactions responsible for the adhesive properties of the mixture. This is consistent with our FTIR results, although no chemical bond formation, we still observe adhesive behavior. Through uniaxial and shear mechanical testing, both simulations (Figs. 2l-o, supporting video SV6-7) and experiments (Figs. 1i-l) quantitatively and qualitatively show a superior adhesive nature of the mix of PDMS and PTFE over PDMS alone. The discrepancy between calculated and experimental stress-strain relations can be ascribed to the discrepancy between experimental and computational models. Due to limitations of computational resources, the computation has to rely on the assumption of periodic boundary conditions unlike experimental samples.

Indeed, periodic boundary conditions allow for an infinitely periodic structure to be treated computationally as a unit small enough to fit into the available computational resources and big enough for boundaries not to directly interact with each other. While this necessary computational assumption is qualitatively reliable for both crystalline and non-crystalline structures, it tends to be more quantitatively reliable for crystalline structures than non-crystalline structures like the PDMS/PTFE polymer composite.

Furthermore, while experimental samples likely contain a certain amount of impurities including defects, the computational models do not. The absence of defects in the computational model is crucial for the compression/tension tests performed in this work in that, even the smallest amount of impurities could result in a significant impact in the recoverability of the material. It is therefore expected that a defect-free computational model quantitatively outperforms a defected experimental sample. Since the real sample has irregularities that are difficult to characterize and accurately reproduce in simulations, the comparison between our

simulations and experiments is intended to be mostly qualitative. Our simulations therefore serve the purpose of confirming qualitative trends and shedding light on the chemical interactions responsible for both the samples' recoverability and adhesive property.

The very high electronegativity difference is deemed the primary cause of the aforementioned reformable and strong interfacial bonding as evinced by the shear mechanical testing (Fig. 2n for simulations and Figs. 1i-k for experiments), the lack of evidence for covalent bonding in STM data, and the diametrically opposed polar nature of fluorine and hydrogen atoms.

Additional theoretical simulations of the PTFE/PDMS mixture show that the gluing mechanism proposed above doesn't just work within the components of the mixture, but also between the mixture and an external material in presence and in absence of water, a comparable stress-strain relationship was computed on two structures obtained by sandwiching a chunk of the PTFE/PDMS mixture between two Si (100) substrates in presence and in absence of water (see Fig. 3). The adhesion between the Si (100) substrates and the PTFE/PDMS mixture remains throughout the unloading process (with and without water), thereby testifying to the gluing capability of the PTFE/PDMS mixture to the Si (100). The Si (100) and PTFE/PDMS adhesive interfaces at the end of the unloading stage, zoomed in at the bottom of Fig. 3a, are evincive of the lingering interfacial bonding (between PDMS and PTFE chains as well as the blend and the Si) described above both in the presence and in absence of water (Supporting video V7).

Moreover, the chemical affinity between PDMS and PTFE is shown by both constructive orbital overlaps and electrostatic attractions between PDMS hydrogen atoms and PTFE fluorine atoms. Indeed, PDMS and PTFE trinomers in Fig. 3b are designed to probe the affinity between the middle monomers of both trinomers and show, in their optimized respective geometries, that

PDMS hydrogen atoms from methyl groups (-CH_3) and fluorine atoms from PTFE stick out. They are therefore likely responsible for the interaction between both polymers. This is confirmed by the big red and blue HOMO lobes (highest occupied molecular orbitals) around PDMS methyl groups' hydrogen atoms constructively overlapping with the big red and blue LUMO lobes (lowest unoccupied molecular orbitals) around PTFE fluorine atoms, respectively (Fig. 3c). The electrostatic potentials in Fig. 3d further shed light on the affinity between PDMS and PTFE through the very strong negative charges around fluorine atoms on PTFE (red areas) facing the very strong positive charges around hydrogen atoms on PDMS (blue areas) testifying to the previously argued electronegativity difference. Extending the constructive orbital overlap and electrostatic attraction shown in Figs 3c-d from trinomers to much longer polymer chains provides the strong, yet flexible, interfacial attraction between PDMS and PTFE responsible for the superior mechanical properties shown both in experiments and in molecular dynamics simulations. Interactions between substrate surfaces which can have either reactive sites or loose charges help the adhesive adhere to substrates and the flexibility of the dipole interactions allows the bonds to easily reform thus enabling the adhesive to be reused multiple times while maintaining its adhesive properties.

The use of liquid polymers allows the polymer chains to easily re-arrange and create the strongest adhesive configuration while aiding in the contact between substrates. This methodology promotes adhesion through molecular-level dipole interactions, which are repeated throughout the polymer chains. The proposed adhesive defines a unique category of reversible, instant biocompatible (Fig.S14, Supporting information) adhesives that work in both humid and dry environments, a combination of properties that we have not seen before. Based on theoretical

and experimental pieces of evidence, these adhesives could be categorized as viscoelastic adhesives.

Acknowledgements

The authors gratefully acknowledge funding support from the Air Force Office of Scientific Research (FA9550-13-1-0084). We would also like to acknowledge DuPont for providing free samples of Zonyl 1000 MP for research purposes.

References

[1] E.A. Appel, O.A. Scherman, Gluing gels: A nanoparticle solution, Nat. Mater. 13 (2014) 231–232.
[2] Z. Cao, A. V. Dobrynin, Nanoparticles as Adhesives for Soft Polymeric Materials, Macromolecules. 49 (2016) 3586–3592.
[3] P.J. Cole, R.F. Cook, C.W. Macosko, Adhesion between Immiscible Polymers Correlated with Interfacial Entanglements, Macromolecules. 36 (2003) 2808–2815.
[4] C.R. Matos-Pérez, J.D. White, J.J. Wilker, Polymer composition and substrate influences on the adhesive bonding of a biomimetic, cross-linking polymer, J. Am. Chem. Soc. 134 (2012) 9498–9505.
[5] H. Yuk, T. Zhang, S. Lin, G.A. Parada, X. Zhao, Tough bonding of hydrogels to diverse non-porous surfaces, Nat. Mater. 15 (2015) 190–196.
[6] N.S. Pesika, H. Zeng, K. Kristiansen, B. Zhao, Y. Tian, K. Autumn, J. Israelachvili, Gecko adhesion pad: a smart surface?, J. Phys. Condens. Matter. 21 (2009) 464132.
[7] H. Lee, B.P. Lee, P.B. Messersmith, A reversible wet/dry adhesive inspired by mussels and geckos, Nature. 448 (2007) 338–341.
[8] C. Zhong, T. Gurry, A. a Cheng, J. Downey, Z. Deng, C.M. Stultz, T.K. Lu, Strong underwater adhesives made by self-assembling multi-protein nanofibres, Nat. Nanotechnol. 9 (2014) 858–866.
[9] D.M. Drotlef, L. Stepien, M. Kappl, W.J.P. Barnes, H.J. Butt, A. Del Campo, Insights into the adhesive mechanisms of tree frogs using artificial mimics, Adv. Funct. Mater. 23 (2013) 1137–1146.
[10] P.G. Lawrence, Y. Lapitsky, Ionically cross-linked poly(allylamine) as a stimulus-responsive underwater adhesive: Ionic strength and pH effects, Langmuir. 31 (2015) 1564–1574.
[11] S. Plimpton, Fast Parallel Algorithms for Short-Range Molecular Dynamics, J. Comput. Phys. 117 (1995) 1–19.
[12] S. Goverapet Srinivasan, A.C.T. Van Duin, Molecular-dynamics-based study of the collisions of hyperthermal atomic oxygen with graphene using the ReaxFF reactive force field, J. Phys. Chem. A. 115 (2011) 13269–13280.
[13] K. Chenoweth, A.C.T. van Duin, W.A. Goddard, ReaxFF Reactive Force Field for

Molecular Dynamics Simulations of Hydrocarbon Oxidation, J. Phys. Chem. A. 112 (2008) 1040–1053.
[14] K. Chenoweth, S. Cheung, A.C.T. Van Duin, W.A. Goddard, E.M. Kober, Simulations on the thermal decomposition of a poly(dimethylsiloxane) polymer using the ReaxFF reactive force field, J. Am. Chem. Soc. 127 (2005) 7192–7202.
[15] M.D. Hanwell, D.E. Curtis, D.C. Lonie, T. Vandermeerschd, E. Zurek, G.R. Hutchison, Avogadro: An advanced semantic chemical editor, visualization, and analysis platform, J. Cheminform. 4 (2012).
[16] M.J. Frisch, G.W. Trucks, H.B. Schlegel, G.E. Scuseria, M.A. Robb, J.R. Cheeseman, G. Scalmani, V. Barone, B. Mennucci, G.A. Petersson, H. Nakatsuji, M. Caricato, X. Li, H.P. Hratchian, A.F. Izmaylov, J. Bloino, G. Zheng, J.L. Sonnenberg, M. Hada, M. Ehara, K. Toyota, R. Fukuda, J. Hasegawa, M. Ishida, T. Nakajima, Y. Honda, O. Kitao, H. Nakai, T. Vreven, J.A. Montgomery, Gaussian 09, Revision B.01, Gaussian 09, Revis. A.1, Gaussian, Inc., Wallingford CT. (2009).
[17] A.D. Becke, Density-functional exchange-energy approximation with correct asymptotic behavior, Phys. Rev. A. 38 (1988) 3098–3100.
[18] W.J. Hehre, R. Ditchfield, J.A. Pople, Self—Consistent Molecular Orbital Methods. XII. Further Extensions of Gaussian—Type Basis Sets for Use in Molecular Orbital Studies of Organic Molecules, J. Chem. Phys. 56 (1972) 2257–2261.
[19] H. V Vinters, K. a Galil, M.J. Lundie, J.C. Kaufmann, The histotoxicity of cyanoacrylates. A selective review., Neuroradiology. 27 (1985) 279–291.
[20] L. Montanaro, C.. Arciola, E. Cenni, G. Ciapetti, F. Savioli, F. Filippini, L.. Barsanti, Cytotoxicity, blood compatibility and antimicrobial activity of two cyanoacrylate glues for surgical use, Biomaterials. 22 (2000) 59–66.
[21] K. Kendall, Adhesion: molecules and mechanics., Science. 263 (1994) 1720–5.
[22] K.R. Aguiar, V.G. Santos, M.N. Eberlin, K. Rischka, M. Noeske, G. Tremiliosi-Filho, Efficient green synthesis of bis(cyclic carbonate)poly(dimethylsiloxane) derivative using CO2 addition: a novel precursor for synthesis of urethanes, RSC Adv. 4 (2014) 24334–24343.
[23] C.P. Ennis, R.I. Kaiser, Phys. Chem. Chem. Phys. 12 (2010) 14884.
[24] D.D. Fazullin, G.V. Mavrin, M.P. Sokolov, & Ildar, G. Shaikhiev, Infrared Spectroscopic Studies of the PTFE and Nylon Membranes Modified Polyaniline, Mod. Appl. Sci. 9 (2015) 242–249.
[25] Q. Zhang, J.J. Xu, Y. Liu, H.Y. Chen, In-situ synthesis of poly(dimethylsiloxane)–gold nanoparticles composite films and its application in microfluidic systems, Lab Chip. 8 (2008) 352–357.
[26] T. Uemura, T. Kaseda, Y. Sasaki, M. Inukai, T. Toriyama, A. Takahara, H. Jinnai, S. Kitagawa, Mixing of immiscible polymers using nanoporous coordination templates., Nat. Commun. 6 (2015) 7473.
[27] J.P. Mofokeng, A.S. Luyt, Morphology and thermal degradation studies of melt-mixed poly(hydroxybutyrate-co-valerate) (PHBV)/poly(ε-caprolactone) (PCL) biodegradable polymer blend nanocomposites with TiO2 as filler, J. Mater. Sci. 50 (2015) 3812–3824.

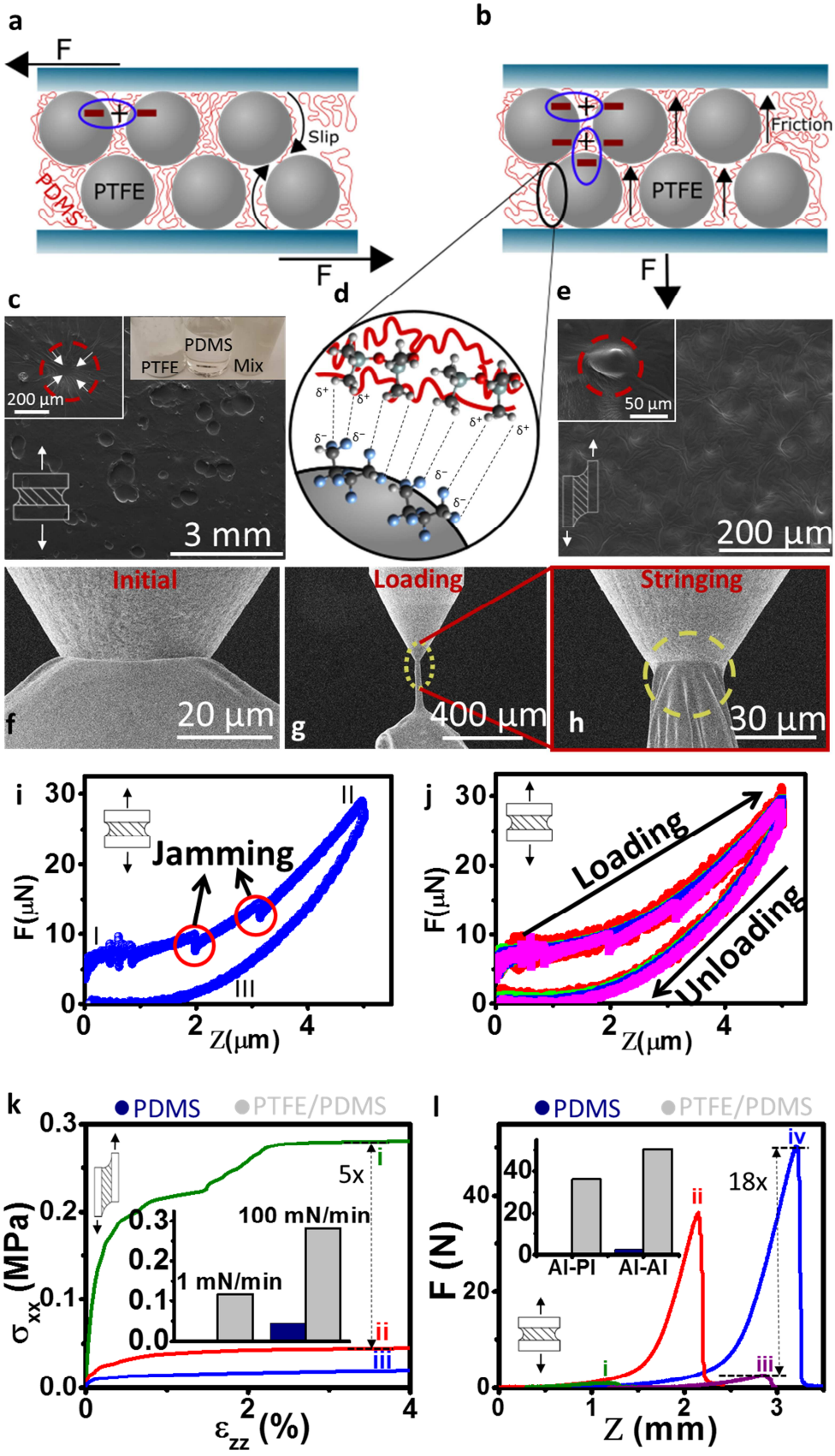
a
F
Slip
PTFE
PDMS
F
d
b
Friction
PTFE
F
c
200 μm
PDMS
PTFE
Mix
3 mm
e
50 μm
200 μm
Initial
Loading
Stringing
f
20 μm
g
400 μm
h
30 μm
i
Jamming
I
II
III
F(μN)
Z(μm)
j
Loading
Unloading
F(μN)
Z(μm)
k
PDMS
PTFE/PDMS
5x
i
100 mN/min
1 mN/min
ii
iii
σxx (MPa)
εzz (%)
l
PDMS
PTFE/PDMS
iv
18x
ii
Al-Pl
Al-Al
i
iii
F (N)
Z (mm)

Figure 1. Proposed Mechanism and SEM Imaging of Failure Modes. The proposed failure mechanisms for (**a)**, shear and (**b**), tensile modes show the interactions at play while failure is happening where dipole interactions prevent initial failure and provide mechanical consistency to the PTFE-PDMS system via dipole-dipole and dipole-induced dipole as seen by SEM images (**c**), tensile failure shows the stress lines due to pull out in the inset as well as the voids left from pulling out the PTFE. The dipole interactions are schematically emphasized in (**d**). The stress lines have also been highlighted in (**e)**, and they can also be seen around all the PTFE, which act as anchoring points due to the strength of the dipole interactions. The in-situ testing images were set up to show the **f**, initial and (**g**), loaded states of the PTFE/PDMS. The stress areas from the loading were clearly outlined in (**g),** and the stringing effect can be seen in (**h**). Stress-strain curves showing (**I**), the initial cycle and (**j**), multiple cycles are present and have key features highlighted. The loading and unloading is clearly marked in (**j**), and the jamming can be seen in (**i**). The DMA testing (**k**), shows 0 wt. % PTFE in blue (iii), 25 wt. % PTFE in red (ii), and 50 wt. % PTFE in green (i). The inset in (**k**) shows the effect of rate on the adhesion of PDMS (navy blue) versus the PTFE/PDMS mix (grey). Tensile testing in (**l),** using an ADMET system shows the difference between raw PDMS in adhesion between aluminum substrates and mismatched substrates (aluminum and plastic). Specifically, (i) represents adhesion between aluminum and plastic using PDMS (green), whereas red (ii) represents adhesion between aluminum and plastic using the PTFE/PDMS mix. Meanwhile, (iii, in purple) represents PDMS adhesion between aluminum substrates whereas (iv, in blue) represents using the PTFE/PDMS mix with aluminum substrates.

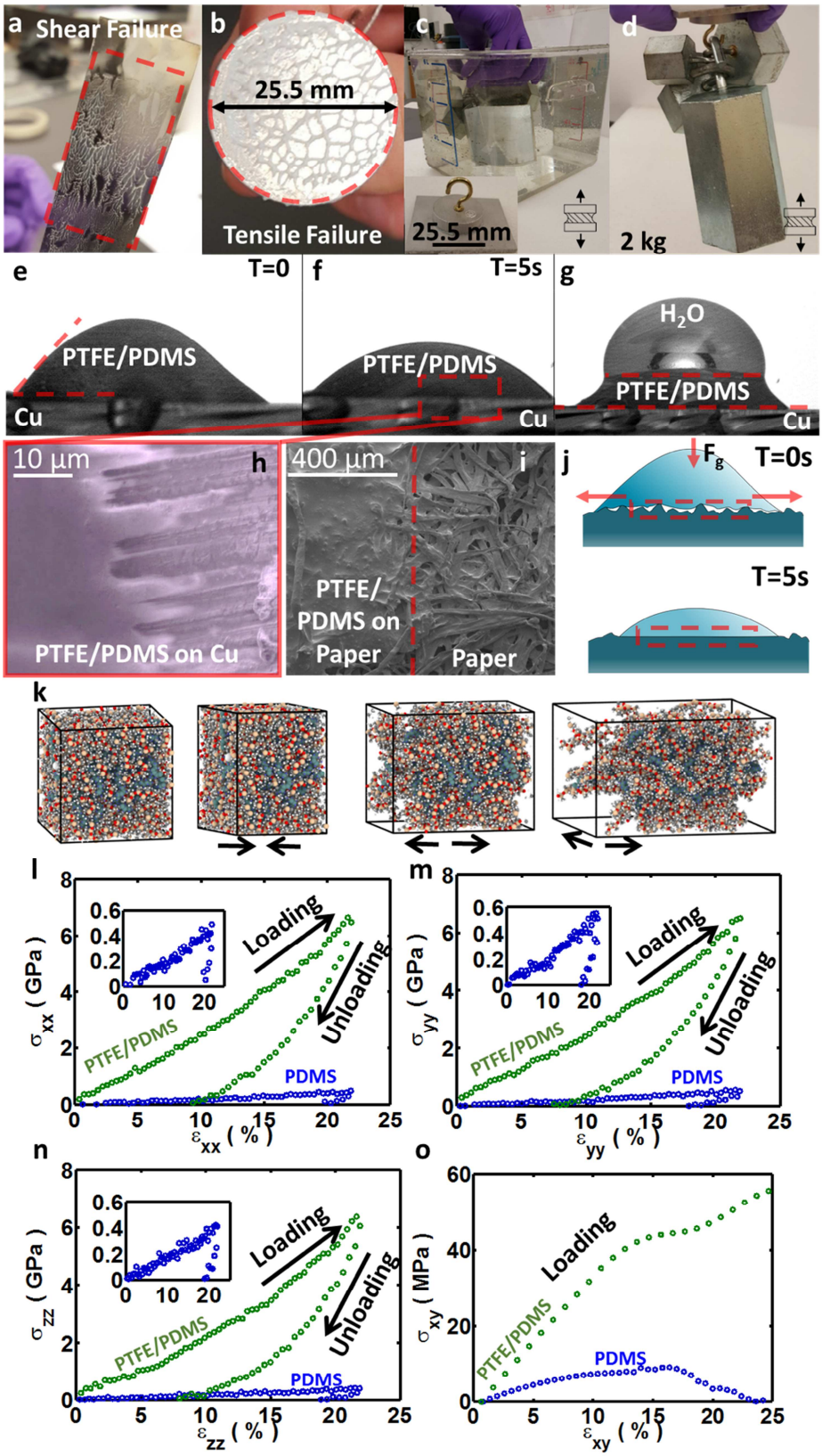
a
Shear Failure
b
25.5 mm
Tensile Failure
c
25.5 mm
d
2 kg
e
T=0
PTFE/PDMS
Cu
f
T=5s
PTFE/PDMS
Cu
g
H2O
PTFE/PDMS
Cu
10 μm
h
PTFE/PDMS on Cu
400 μm
i
PTFE/
PDMS on
Paper
Paper
j
Fg
T=0s
T=5s
k
l
m
n
o
Loading
Unloading
PTFE/PDMS
PDMS
σxx (GPa)
εxx (%)
σyy (GPa)
εyy (%)
σzz (GPa)
εzz (%)
σxy (MPa)
εxy (%)

Figure 2. Mechanical Properties of PTFE/PDMS Blend. The (**a**), shear and (**b**), tensile failure images exhibit expected patterns for slip and pull out cohesive failure, respectively. The blend is used to attach two plates and can sustain approximately 2 kg of weights in air and water (c) and (d). The contact angle of the PTFE/PDMS onto a piece of copper substrate (**e**) and (**f**), The hydrophobicity of the material on copper as shown in (**g**) by placing a drop of water onto a copper substrate that had PTFE/PDMS on it. The copper surface is completely covered by PTFE/PDMS as shown by SEM (**h**). Stronger adhesion of PTFE/PDMS is shown by filling the empty spaces in a paper (i). This mechanism is schematically shown in (**j**). As time passes the liquid polymer phase can relax and spread across the surface, thus filling all the available cracks and pores and promoting better adhesion and allowing it to work with a myriad of surfaces. (**k**), Snapshots of simulation box in biaxial, compressive, and tensile loading for PTFE/PDMS can be seen at the bottom. Uniaxial stress-strain curves for compressive loading and tensile unloading in the: (**l**), x-direction, (**m**)**,** y-direction, (**n**)**,** z-direction, and (**o**)**,** the xy-direction.

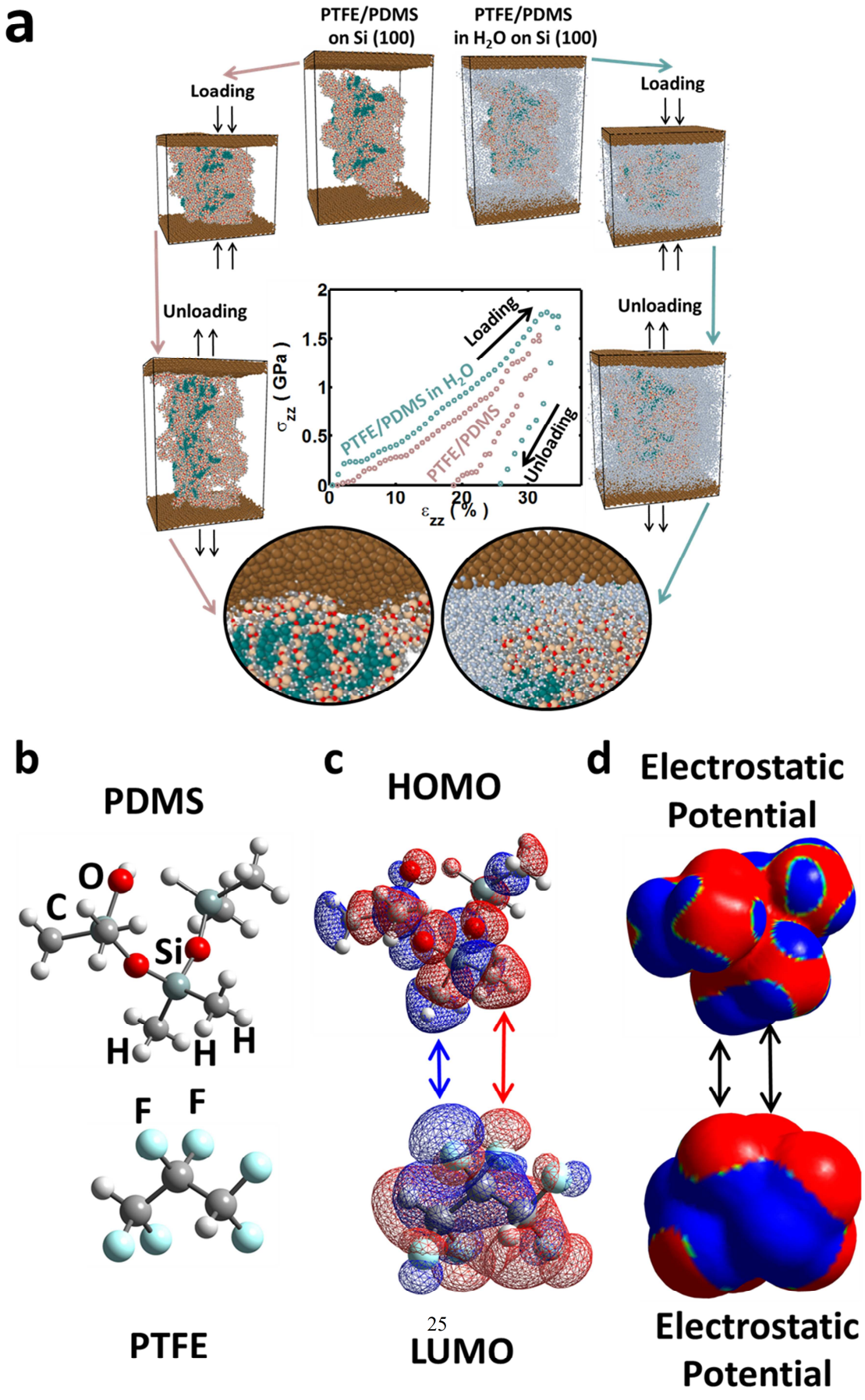
a
PTFE/PDMS on Si (100)
PTFE/PDMS in H2O on Si (100)
Loading
Loading
Unloading
Unloading
PTFE/PDMS in H2O
PTFE/PDMS
Loading
Unloading
σzz (GPa)
εzz (%)
b
PDMS
O
C
Si
H
H
H
F
F
PTFE
c
HOMO
LUMO
d
Electrostatic Potential
Electrostatic Potential

Figure 3. Molecular dynamics simulations of PTFE/PDMS blend PTFE/PDMS on Si (100) substrate in the presence (right) and absence of water (left): (**a**) With respect to initial stages, respective unloading stages show the PTFE/PDMS mixture sticking to Si (100). Stress-strain ($\sigma_{zz}/\varepsilon_{zz}$) curves in the z-direction (center) confirm the gluing capability of the mixture to Si (100) in the presence and absence of water. The interfaces between Si (100) substrate and PTFE/PDMS the blend in the presence (bottom right) and absence (bottom left) of water are zoomed in to further elucidate the adhesive properties of the mixture. The ab initio analysis of PDMS/PTFE chemical affinity shows (**b**), Optimized PDMS ($[C_2H_6OSi]_3$) and PTFE ($[C_2F_4]_3$) hydrogen-passivated trinomers with both middle monomers sticking out of the chain. (**c**)**,** PDMS HOMO and PTFE LUMO constructive orbital overlap indicated by blue and red arrows. (**d**)**,** Electrostatic attraction between PDMS methyl groups' hydrogen atoms (blue positive charges) and PTFE fluorine negative charges (red negative charges). Both electrostatic potentials range from -0.002 (red) to +0.002 (blue) Mulliken units.

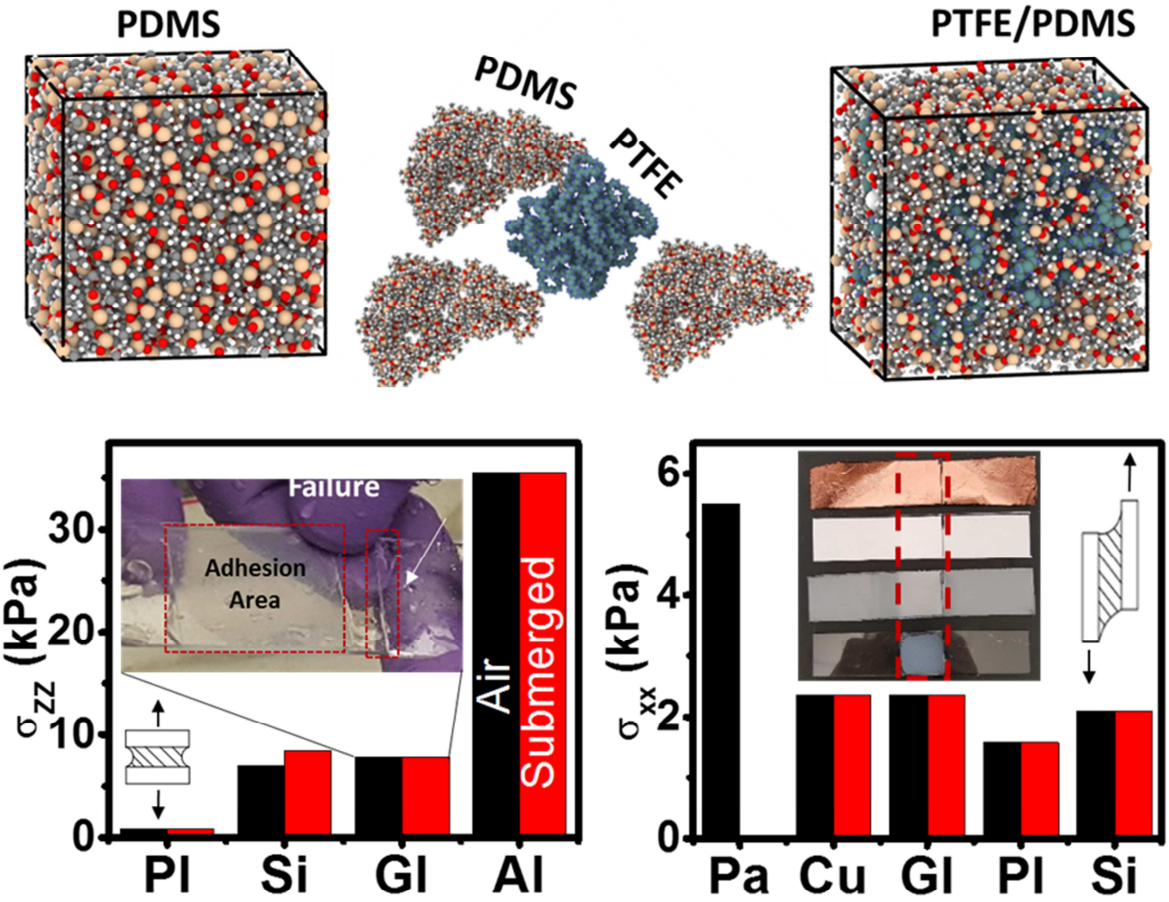
PDMS
PDMS
PTFE
PTFE/PDMS
Failure
Adhesion
Area
Air
Submerged
σ_{zz} (kPa)
0
10
20
30
Pl
Si
Gl
Al
σ_{xx} (kPa)
0
2
4
6
Pa
Cu
Gl
Pl
Si